Talanta 225 (2021) 121982

Contents lists available at ScienceDirect

Talanta

journal homepage: www.elsevier.com/locate/talanta

A sensitive spectrophotometric ellipsometry based Aptasensor for the vascular endothelial growth factor detection

Ishak Afsin Kariper [a], Zafer Üstündağ [b], Mustafa Oguzhan Caglayan [c,*]

[a] Erciyes University, Faculty of Education, 38039, Kayseri, Turkey
[b] Dumlupinar University, Chemistry Department, 43100, Kütahya, Turkey
[c] Bilecik Seyh Edebali University, Bioengineering Department, Bilecik, 11120, Turkey

ARTICLE INFO

Keywords:
Aptamers
Biosensors
Breast cancer
Spectroscopic ellipsometry
VEGF

ABSTRACT

A sensitive and selective, aptamer and spectroscopic ellipsometry based sensor is reported here for the early diagnosis of breast cancer, which is a common type of cancer following lung cancer. It was aimed to develop a single-step and label-free assay for the sensitive and selective detection of $VEGF_{165}$. To this end, two different aptamers and spectroscopic ellipsometry were used. In the presented study, by determining the appropriate aptamer immobilization conditions, the spectroscopic ellipsometry technique was successfully applied for the detection of $VEGF_{165}$ at the range of 1 pM–1000 pM in the buffer. Aptasensors have a detection limit of 5.81 pM and 4.29 pM, respectively.

1. Introduction

Cancer, a complex disease group characterized by uncontrolled growth and spread of abnormal cells, has long been one of the primary causes of death [1]. Early and accurate detection of cancer is extremely important for clinical diagnosis, effective patient follow-up, and, consequently, successful treatment of cancers. A biomarker is defined as "a substance or activity that can be objectively measured and evaluated as an indicator for pharmacological responses to a normal biological process, pathogenic process, or a therapeutic intervention" [2]. Cancer biomarkers are found in tumor tissues or serum and cover a wide variety of molecules, including DNA, mRNA, enzymes, metabolites, transcription factors, and cell surface receptors [3,4]. In the past few decades, significant progress has been made in biomarker detection. Various detection methods have been developed based on the specific recognition of cancer biomarkers such as polymerase chain reaction (PCR) [5], enzyme-linked immunosorbent analysis (ELISA) [6–8], electrophoresis [9], surface plasmon resonance (SPR) [10–13], surface-enhanced Raman spectroscopy (SERS) [14], microcantilever [15], colorimetric analysis [16,17], electrochemical analysis [18–20], field-effect transistors (FET) [21–23], and fluorescent methods [24–26].

Certain nucleic acid sequences, called aptamers, are structures that have unique binding properties for their targets. Aptamers, first reported by Ellington and Gold, are single-stranded DNA, RNA, or peptide sequences and can be specifically bound to targets by folding into certain three-dimensional structures [27,28]. Since their discovery, aptamers have attracted great interest from researchers in the design of biosensors, target imaging agents, and drug delivery. In theory, aptamers can be selected for any particular target [29,30]. To date, high-affinity aptamers have been selected for a wide variety of target molecules, including metal ions, peptides, drugs, proteins, and even whole cells or viruses [31–36].

Due to the unique properties of aptamers, many important applications have been reported for bioanalysis, biomedicine, and especially cancer-related research (cancer biomarker discovery, imaging, diagnosis, and treatment) [37,38]. Numerous aptamers have been developed against cancer-related proteins, such as platelet-derived growth factor (PDGF), vascular endothelial growth factor (VEGF), tenascin-C, nuclear factor kappa light chain enhancer (NFκB), and prostate-specific membrane antigen (PSMA) [39,40].

Optical biosensors for the detection of cancer-related biomarkers and cancer cells using aptamers are generally produced using fluorescence methods due to their high sensitivity. For example, an optical aptasensor assay (5 pM LOD) for $VEGF_{165}$ detection [41], an aptasensor (1.25 pM LOD) for $VEGF_{165}$ detection [42], differentiation of Toledo, CEM, and Ramos cancer cells with silica nanoparticles and aptamers [43], CCRF-CEM cell determination studies using magnetic nanoparticle-containing aptamers [44], and detection and isolation of cancer cells using hairpin-shaped oligonucleotide and silver

* Corresponding author.
E-mail addresses: caglayanmoguzhan@gmail.com, oguzhan.caglayan@bilecik.edu.tr (M.O. Caglayan).

https://doi.org/10.1016/j.talanta.2020.121982
Received 4 August 2020; Received in revised form 2 December 2020; Accepted 5 December 2020
Available online 9 December 2020

Abbreviations and symbols

AFM	Atomic force microscope
Anti-VEGF1	$VEGF_{165}$ specific aptamer #1
Anti-VEGF2	$VEGF_{165}$ specific aptamer #2
BSA	Bovine serum albumin
CRET	Chemiluminescence resonance energy transfer
CTRL	Control aptamer
ECL	Electrochemilimunescence
EDAC	1-ethyl-3-(3-dimethylaminopropyl) carbodiimid
EIS	Electrochemical impedance spectroscopy
ELISA	Enzyme-linked immunosorbent assay
FET	Field-effect transistor
FRET	Fröster resonance energy transfer
HER2	Human epidermal growth factor receptor 2
HIV-1	Human immunodeficiency virus – Type 1
LOD	Limit of detection
MMP	Matrix metalproteinase
MPTES	Mercaptopropyl triethoxysilane
MUA	Mercapto undecanoic acid
MUC1	Mucin1
PBS	Phosphate buffer saline
PCR	Polymerase chain reaction
PSA	Prostate-specific antigen
PSMA	Prostate-specific membrane antigen
PTGF	Protein transforming growth factor
QCM	Quartz crystal microbalance
QRET	Quenching resonance energy transfer
RMS	Root mean square
SE	Spectrophotometric ellipsometry
SELEX	Systematic evolution of ligands by exponential enrichment
SERS	Surface-enhanced Raman spectroscopy
SPE	Screen-printed electrode
SPR	Surface plasmon resonance
$VEGF_{165}$ or VEGF	Vascular endothelial growth factor
VOC	Volatile organic compounds
Δ	Delta, ellipsometric parameter, phase shift
Ψ	Psi, ellipsometric parameter, intensity change at polarization states

nanostructures [45] can be found in the literature. Besides fluorescent aptasensors, colorimetric and Raman aptasensors are also available in the literature for the detection of cancer-related biomarkers [46,47]. Electrochemical sensors are also used for the precise detection of cancer-dependent biomarkers and cancer cells due to their high sensitivity, low cost, and clinical application potential [48]. Electrochemical aptasensors have been produced for human epidermal growth factor receptor 2 (HER2) [49] and Mucin1 (MUC1) [50]. Lee et al. performed the electrochemical determination of VEGFs (100 pM LOD) using anti-VEGF aptamer modified silicon nanowire field-effect transistors (SiNW-FETs) [51].

Over the past decade, a better understanding of carcinogenesis and tumor metastasis has demonstrated the ability of tumor cells to form new vasculatures to receive a large number of nutrients and oxygen necessary for growth [52,53]. The main protein mediator of this process is Vascular Endothelial Growth Factor, also known as VEGF [54,55]. As a result of the insufficient supply of nutrients and oxygen to tumor cells, $VEGF_{165}$ is over-expressed to form veins and provide a growing vascular network [56]. Thus, the concentration of $VEGF_{165}$ in the blood increases (higher than 1 ng/mL) [57]. Until now, a relationship has been established between serum $VEGF_{165}$ levels and cancer in various cancer types [58–60] such as cervical cancer [61], hepatocellular carcinoma [62], and breast cancer [63]. $VEGF_{165}$ is also a signal protein used as a serum biomarker in some human diseases, such as rheumatoid arthritis [64], psoriasis [65], and profiling vitreoretinopathy [66]. Existing methods used for $VEGF_{165}$ determination include immunohistochemistry, ELISA, radioimmunoassay, and Western blot [67].

An important characteristic of a biosensor is its detection limit (as well as sensitivity). This is a variable that depends much more on the type of transducer, as well as on the interaction of the bioreceptor and the target. Spectrophotometric ellipsometry (SE), which offers a successful performance in terms of detection limit, has become a widely used and preferred method [68]. The SE method is used to examine thin films in any medium. With this method, film parameters, film thickness, composition, optical properties, and surface structure can be examined [69]. SE is based on measuring the polarization change obtained by the reflection of the polarized monochromatic light plane wave from a surface at a certain angle [70,71]. Psi (Ψ) and Delta (Δ) parameters measured by ellipsometer are called ellipsometric angles and can be described as experimentally obtained data from an ellipsometer [72]. Since the mentioned ellipsometric parameters are very sensitive to changes in the surface, the interaction of aptamers with the target molecule immobilized on a base material will cause changes in Psi (Ψ) and Delta (Δ) values. In particular, the Delta (Δ) parameter is very sensitive to the change in dielectric constants in any thin film. Our group has different studies evaluating the performance of ellipsometry in different analytes. The use of aptamer and ellipsometry has been reported in subjects such as determination of aminoglycoside antibiotics from dairy products [73], and HIV-1 Tat protein [74], Influenza A [75], mercuric ion [76], and zearalenone [77] determination.

In this study, the SE method using two different aptamers was developed for VEGF determination.

2. Materials and methods

2.1. General

Unless otherwise stated, all chemicals were of analytical purity and were supplied from the local representative of Sigma-Aldrich. MilliQ water was used for final cleaning and buffer preparation. Distilled water was used for cleaning purposes. Ellipsometric measurements were made using a spectrophotometric ellipsometer (Optosense, S6000, Türkiye). Schematic representation of the analysis method is given in Fig. 1. The thickness of the immobilized layers was measured by ellipsometry using the Si substrate/SiO_2 oxide layer/organic layer modeling. Surface topography and roughness were determined using an atomic force microscope (AFM, Park Systems XE100) in non-contact mode. The concentrations stated in the study indicate the final concentrations. All experiments and measurements were repeated 3 times, unless otherwise specified, to meet analytical requirements.

2.2. Immobilization of aptamers and improvement of immobilization conditions

Anti-VEGF aptamers were supplied amine-functionalized at the 5′ end to be immobilized on the Si-wafers. The anti-VEGF1 [78] aptamer has a sequence of 5′-NH_2-$(CH_2)_6$- CCG TCT TCC AGA CAA GAG TGC AGG G – 3′ (25 bases). The anti-VEGF2 [79] aptamer, which has the same base length as the previous one, has a sequence of 5′-NH_2-$(CH_2)_6$-TGT GGG GGT GGA CGG GCC GGG TAG A-3′. A 24 base length 5′-NH_2-$(CH_2)_6$ -ACG AAG TGA CCC GTT GCC GGT CGA-3′ aptamer was used as a control (CTRL) aptamer. Si-wafers used as sensor chips were immersed in the oxidizing solution consisting of a mixture of H_2SO_4 and H_2O_2 (7:3 by volume) for 2 s before use and then rinsed with

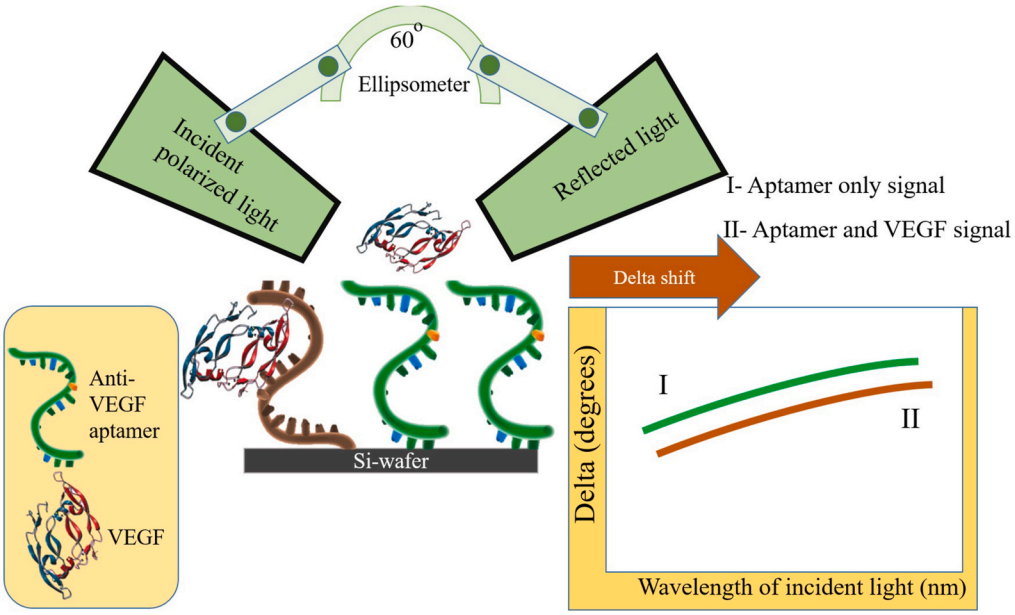

Fig. 1. Schematic representation of the spectrophotometric ellipsometry method.

ethyl alcohol. After this process, the surfaces were cleaned with 100 W oxygen plasma using the Diener model plasma device (Germany) to remove organic residues completely.

Anti-VEGF1, Anti-VEGF2, and CTRL aptamers were immobilized to the surface of the –COOH terminated Si-wafers. The cleaned wafers were kept in oxygen plasma for 30 min for the silanol reaction. Then, mercaptopropyl triethoxysilane (MPTES), prepared in absolute ethyl alcohol, was used to obtain a –SH terminated functional surface on the Si-wafers. MPTES concentration and reaction time optimization was done by measuring the ellipsometric thickness during the MPTES layer creation phase. Then, using the disulfide reaction, –COOH functional ends were formed on the Si-wafer surface with mercapto undecanoic acid (MUA). At this stage, the layer formation process was followed by measuring the ellipsometric thickness and optimum parameters were determined in this way. The aptamers having the NH_2-functional group were then immobilized to the –COOH functionalized Si surface by a 1-ethyl-3- (3-dimethyl aminopropyl) carbodiimide (EDAC) reaction. Aptamers were prepared in 100 mM phosphate buffer solution (PBS, pH 7) and stored at 4 °C. Aptamer solutions used in the studies were prepared by diluting from the stock solution. In the optimization of the concentration and reaction times, the thickness of the organic accumulation on the Si-wafer surface was determined by the ellipsometric method. Modeling was carried out using the software of the device after ellipsometric measurements and air/organic layer (thickness measured)/SiO_2 layer (5 nm) and Si substrate were used in the model.

2.3. Determination of the analytical performance of $VEGF_{165}$ aptasensor

The analytical performance of the aptamers and control aptamer in $VEGF_{165}$ (will be used as VEGF after this section in the text for clarity) determination was evaluated using a solution of 1.0 pM−500 pM VEGF in the buffer solution. VEGF solutions were prepared using 25 mM Tris – HCl, pH 7.4, 150 mM NaCl, 50 mM KCl buffer. The Si-wafers, which were interacted with the VEGF solution for 30 min, were washed using the buffer solution after this process. The dried wafers were analyzed using a spectroscopic ellipsometer at a 60° light incidence angle using 400–1700 nm monochromatic and polarized light. The ellipsometric parameters, delta (Δ) and psi (Ψ) were obtained, and the delta (Δ) angle, in other words, the phase shift between polarized light and reflected light was preferred as the sensor response, as it is more sensitive to accumulation on the surface. Molecular accumulation on the surface changes the thickness and dielectric function. The Δ spectrum obtained around the wavelength of 450–600 nm shows a near-linear Δ-λ relationship. At the same time, with the accumulation on the surface, it shifts to lower degrees. For this reason, sensor calibration graphs were obtained by using Δ value at this wavelength. Sensitivity and limits of detection (LODs) were calculated using the function graph of the Δ change dependence on VEGF concentration. Bovine serum albumin (BSA) was used to control the specificity of the sensor.

2.4. The ellipsometric thickness and roughness measurements

The thickness of the molecular layer deposited on the surface of each sensor chip was calculated using the equipment's built-in software, using both Δ and Ψ values. All thickness measurements were performed on 10 different randomly selected measuring points on 3 different test samples and reported as the mean value (±1σ). Surface topographic images were taken using ParkSystems XE-100 model atomic force microscope (AFM) device (Suwon, Korea) and roughness analysis was performed using the software of this device. The 512 × 512-pixel topographic images were obtained using a non-contact mode tip (NCM-silicon, Park Systems, Korea). Topographic measurements were also performed on 3 different test samples on 10 different and randomly selected measurement points and reported as the mean value (±1σ).

3. Results and discussions

3.1. Immobilization of aptamers and improvement of immobilization conditions

Immobilization conditions of the MPTES layer on Si-wafer were optimized first. In this immobilization process, adsorption and covalent binding mechanisms are effective on the surface. Both the MPTES concentration and the time it takes for the molecules at a certain concentration to interact with the Si-wafer surface affect the binding mechanism. For this reason, the effect of interaction on surface accumulation at different times in a 1 μM MPTES solution was investigated using an oxygen plasma-treated Si-wafer. After this process, which was carried out between 30 min and 360 min, the surface thickness was measured using an ellipsometer. The wavelength-dielectric constant values of the materials were selected from the device library. As seen in Fig. 2a, the thickness was around 1 nm during the first 120 min. The

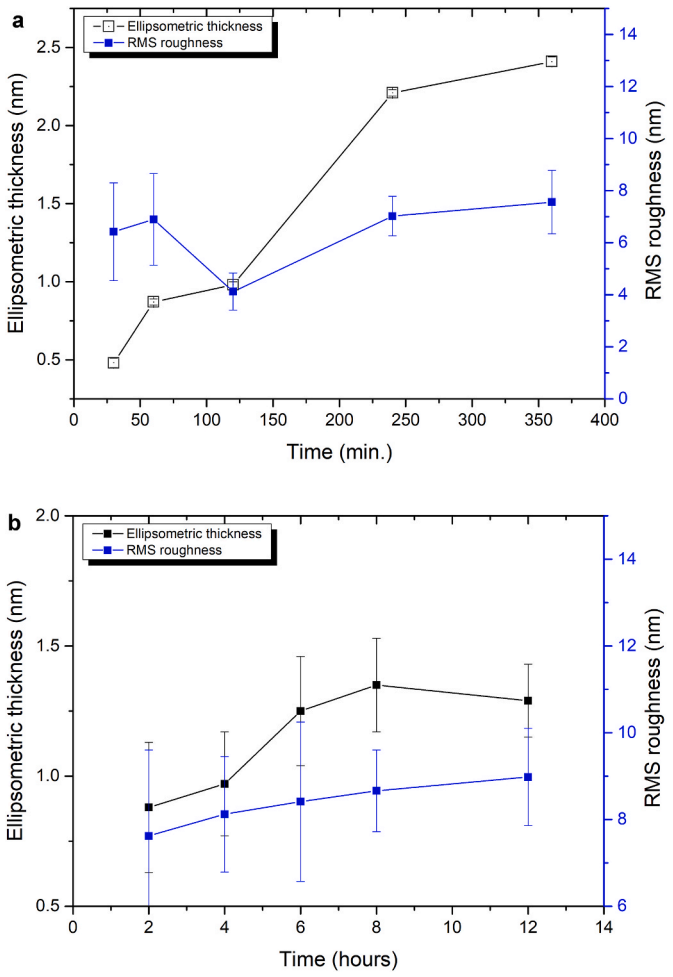

Fig. 2. Surface thickness and RMS roughness change graph for monolayer formation **a)** at 1 μM MPTES, and **b)** 1 μM MUA concentration. (Repetition is 3, ellipsometric measurement and AFM roughness measurement point is 10).

thickness increased to around 2 nm for 240 and 360 min. AFM roughness decreases somewhat around 120 min, indicating that monolayer formation was achieved. Considering the theoretical lengths of MPTES molecules, it can be said that during the first 120 min, formation occurs close to a single layer, and since this time, multiple layers are formed. This situation was supported by the increase in the RMS roughness of the samples after 120 min.

In the process of monolayer formation on the surface by the silanol reaction, it was expected that the thickness should not increase to show more than a single-layer formation. However, this situation has also emerged in our previous studies. The reason for this could be the water molecules adsorbed to the surface as a result of the dissolution of water vapor resulting from the humidity of the air in absolute ethyl alcohol. Although precautions such as drying the Si-wafers, immersion in the solution in ethyl alcohol, and keeping the reaction medium closed, MPTES islets did not be prevented from forming on the surface and accumulation of MPTES units in oligomer form. Although this situation has not been proven by other methods, this has been observed in our previous studies, and AFM topographic images of islet structures were given [76]. Therefore, performing the reaction for 120 min using 1 μM MPTES was considered sufficient and appropriate for the study. The effect of MPTES concentration on monolayer formation has also been previously examined and it is thought that the use of MPTES at 1 μM concentration was sufficient.

After this process, optimization was carried out to create a disulfide bond between the –SH terminated surface and the MUA. For this purpose, the reaction was carried out at room temperature, in the dark, and a closed container purged with nitrogen. Since we determined that the disulfide reaction occurred slowly in our previous studies, it was aimed to perform time optimization by continuing the reaction for 2–12 h. This time, 1 μM MUA (in ethyl alcohol) was prepared for optimization. At the end of the specified period, after the Si-wafers which were previously modified with MPTES were removed and washed with ethyl alcohol, the layer accumulated on the surface was measured using an ellipsometer. Modeling was done with dielectric constants in the library of the device using Δ and Ψ parameters obtained in ellipsometric measurement and organic layer thickness was determined and presented in Fig. 2b. At the end of this process performed to obtain a carboxyl-terminated surface, it is seen that the thickness reaches a plateau after 6 h using 1 μM MUA. RMS roughness values have changed slowly, reaching around 8 nm after 2 h. Within the scope of the study, it was deemed appropriate to perform the reaction for 6 h while the MUA concentration was 1 μM to ensure that the Si-wafer surfaces were uniform in each batch.

Furthermore, the optimums for the binding of aptamers with the EDAC mechanism were determined by measuring the ellipsometric thickness (Table 1). At the immobilization stage of the aptamer of 1.5 μM antiVEGF1, 120 min later, the RMS roughness decreased and the ellipsometric thickness has become steady. For this reason, the optimum binding time and concentration of both aptamers with the same length were determined as 120 min and 1.5 μM.

3.2. Analytic performance of the spectrophotometric ellipsometric sensor

The interaction between VEGF solution in buffer and anti-VEGF1, anti-VEGF2, and CTRL aptamers was investigated using SE. For this purpose, the angle of incident light was brought to 60° and delta variation between 400 nm and 1700 nm was examined. The sensor response obtained as a result of the interaction of VEGF solution (1–1000 pM) prepared in the buffer with the sensor chip is given in Fig. 3a and b. As can be seen, the sensor response from each sensor chip was similar to each other (since the substrate is Si-wafer and the top layer is an organic material), and the sensor response shifted to lower Δ degrees with the increasing VEGF concentration. When this change was examined for VEGF solution prepared from 10 pM to 1000 pM, it was observed that the Δ-λ change around the wavelength of 450–600 nm was linear with a determination coefficient of 0.96–0.98 (R^2). By considering the linear region in this range, the relative sensor response (based on the buffer-only signal) was calculated and the sensor calibration graphs were plotted (Figure 4a and b).

Calibration curve parameters of anti-VEGF1 and anti-VEGF2 aptamers and the detection limits calculated with 3σ are given and compared in Table 2, taking 3 times the standard deviation obtained at the lowest VEGF concentration (e.g. S/N ratio being 3).

The CTRL aptamer gave a 1.33 ± 0.41 Δ change when using 10 pM VEGF while causing a sensor signal of 1.76 ± 0.52 Δ when using 100 pM VEGF, and 1.64 ± 0.48 Δ degrees when using 1000 pM VEGF. This shows that the aptamers are selective, but a very low amount of VEGF cannot be removed from the sensor surface during the washing.

As seen in Fig. 4, the interaction between VEGF and anti-VEGF corresponds to the coupling reaction of the analyte with single or multiple

Table 1
Ellipsometric layer and roughness measurements for 1.5 μM Anti-VEGF1 immobilization (n = 10).

Time (min.)	Thickness (nm)	Roughness (nm)
30	1.08 ± 0.34	7.26 ± 2.11
60	1.98 ± 0.29	8.68 ± 2.76
120	3.11 ± 0.32	6.86 ± 1.77
240	3.41 ± 0.31	7.04 ± 1.86
360	3.71 ± 0.33	6.89 ± 1.98

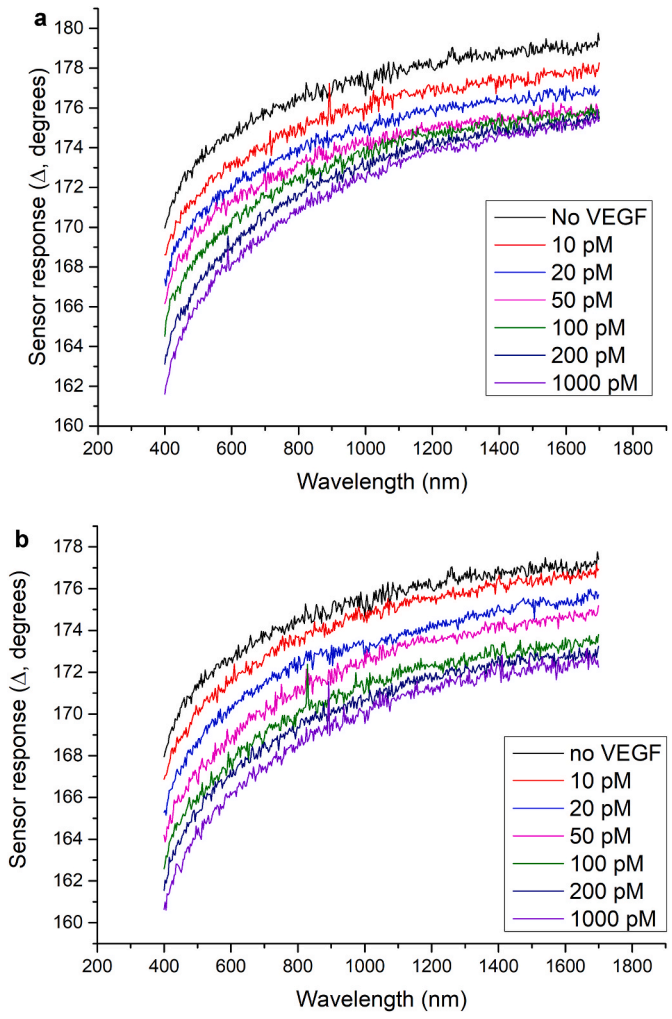

Fig. 3. a) Anti-VEGF1 and **b)** anti-VEGF2 aptamer sensor responses obtained with 10–1000 pM VEGF.

Table 2
Analytical performances of aptasensors (n = 3).

Aptamer	Parameters	R^2	3σ	LOD (S/N = 3)
Anti-VEGF1	Slope = 5.09618 Intercept = -3.02429	0.97	0.87	5.81 pM
Anti-VEGF2	Slope = 3.91953 Intercept = −1.24733	0.98	1.23	4.29 pM

sites and shows a semi-logarithmic relationship. The relationship between the log VEGF concentration and the sensor signal (i.e. Δ exchange) was linear with a high R^2. The calibration curve fit the Δ = 5.096log [VEGF]-3.024 linear function (0.97 R^2). The sensitivity of the anti-VEGF1 sensor by spectroscopic ellipsometry was 5.096 Δ/log [VEGF]. Similarly, the calibration curve for the anti-VEGF2 fit the Δ = 3.9195log [VEGF]-1.2473 linear function with a 0.98 coefficient of determination. The sensitivity of the anti-VEGF2 sensor by spectroscopic ellipsometry was also 3.9195 Δ/log [VEGF].

The compatibility of the calibration data to the Langmuir model was also checked, considering the aptamer- VEGF interaction takes place in a single available aptamer region, on the sensor surface. As can be seen in Fig. 5, the anti-VEGF aptamer/VEGF interactions fit the Langmuir model given in Equation (1) with R^2 of 0.97 and 0.98, respectively.

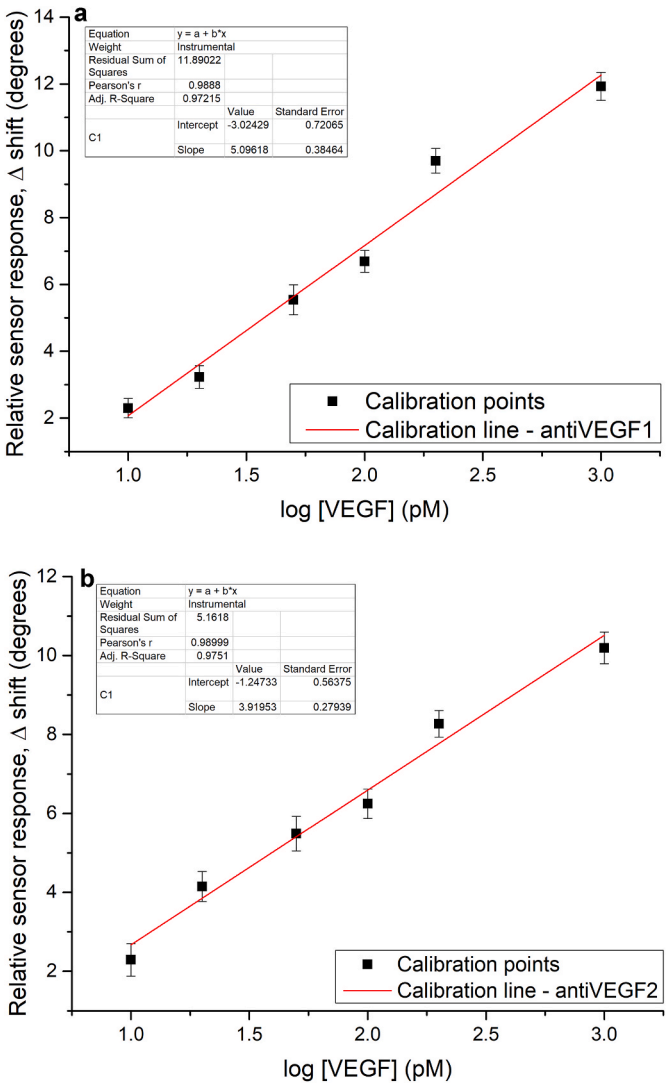

Fig. 4. Calibration curve of **a)** anti-VEGF1 aptamer, and **b)** anti-VEGF2 aptamer.

$$\Delta = \frac{ab[VEGF]^{1-c}}{1 + b[VEGF]^{1-c}} \quad \text{Eq.1}$$

Langmuir model coefficients are given in Table 3. It has been determined that the sensitivity of the anti-VEGF1 sensor is higher than that of the anti-VEGF2 sensor. This can be confirmed by comparing the interaction between aptamer and VEGF based on the Langmuir coefficients. As can be seen in Table 3, the product of parameters **a** and **b** is 0.76 for the anti-VEGF1 model and 0.43 for the anti-VEGF2 model. There is a difference of approximately 50% between the **c** coefficient of the Langmuir model (Table 3). However, both aptasensors reached approximately the same limit of detection (Table 2). Although there is a 50% difference in the Langmuir **c** parameter, it can be said that the two data are close to each other in terms of magnitude. For this reason, it was concluded that the anti-VEGF1 and anti-VEGF2 aptamers have approximately the same affinity to the VEGF. The limit of detection of both aptamer, which was similar in terms of length (25 bases), was found to be 5.81 and 4.29 pM, respectively. Besides, the interaction between aptamer and VEGF fits the Langmuir model with a very high coefficient of determination as expected and confirmed the single site (1 aptamer - 1 VEGF) relationship.

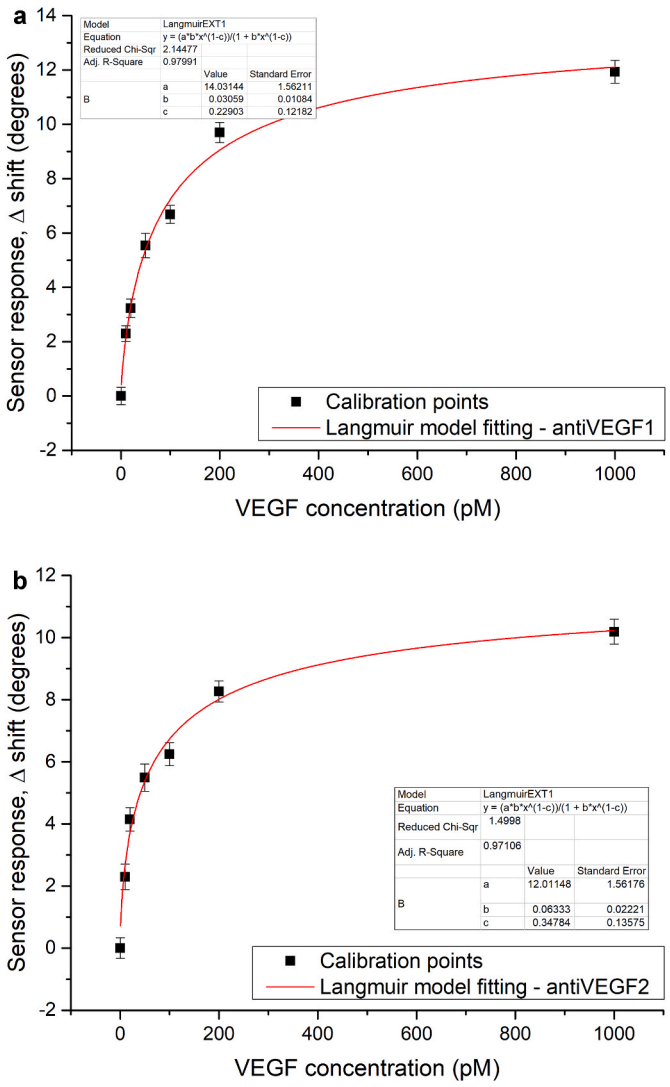

Fig. 5. The Langmuir model fitting for aptamer – VEGF interaction.

Table 3
Langmuir model fitting and model parameters for anti-VEGF1 and anti-VEGF2 aptasensors (n = 3).

Parameters of the Langmuir model			Regression coefficient (R^2)
Anti-VEGF1	A	12.011	0.97
	B	0.063	
	C	0.348	
Anti-VEGF2	A	14.031	0.98
	B	0.031	
	C	0.229	

3.3. The specificity of the aptasensors

To test the specificity of the sensor, 100 pM and 1000 pM bovine serum albumin (BSA) were analyzed solely with anti-VEGF1 and anti-VEGF2 sensors. Also, the analysis was carried out by adding BSA solution in the same proportions as VEGF solution with the final concentration of 100 pM and 1000 pM. The results of the specificity tests are given in Table 4. As can be seen in Table 4, the sensor response obtained for medium and high BSA concentrations for anti-VEGF1 was obtained approximately 3 times the noise obtained for VEGF at that concentration and remained within the 3σ limits. Similarly, the sensor response obtained for anti-VEGF2 was around 3σ at low concentrations but slightly

Table 4
Specificity test results of aptamers for a) BSA only, and b) BSA and VEGF added simultaneously (n = 3).

a) BSA only	BSA spiked (pM)	VEGF spiked (pM)	Sensor response, Δ	S/N ratio
Anti-VEGF1	100	0	0.98 ± 0.11	2.97
	1000	0	1.21 ± 0.29	2.88
Anti-VEGF2	100	0	1.18 ± 0.31	3.19
	1000	0	1.46 ± 0.34	3.65
b) BSA and VEGF	**BSA spiked (pM)**	**VEGF (pM) spiked**	**VEGF found (pM)**	**Recovery (%)**
Anti-VEGF1	100	100	101.6 ± 1.1	101.6
	1000	1000	1029 ± 2	102.9
Anti-VEGF2	100	100	102 ± 1.4	102.0
	1000	1000	1017 ± 2	101.7

increased at high BSA concentration, up to 4 times the noise rate. However, in both cases, it can be said that the response of the sensor remains within the noise limits in the BSA only analysis. The deviation in the sensor response obtained by applying VEGF and BSA solution mixture to the sensor at the same time was less than 3%. It is a known phenomenon that aptamers are specific to their targets and the aptamers used in this study were determined to be specific against VEGF.

4. Conclusions

The diagnosis and monitoring of prognosis of cancer need easy to use, selective, and sensitive sensors to be used in the detection of biomarkers. Although the analytical performance of most sensor platforms developed and reported for this purpose is sufficient, there are still limitations in commercialization. For this reason, testing and reporting the applicability of different platforms in biomarker detection is an important milestone for using these sensor platforms in practice as the main goal. In this study, a spectrophotometric ellipsometry-based VEGF aptasensor has been developed by using two different aptamers based on the detection of VEGF, which has been studied frequently as a biomarker model. The determination of VEGF solutions in the range of 10 pM–1000 pM was successfully performed using two aptamer-based platforms. This range is somewhat wider than those of some aptamer-based VEGF sensors encountered in the literature (Table 5). For instance, the detection range of commercially available ELISA kits is a bit narrower (e.g. 0.25 pM–100 pM). In some types of cancer, the physiological range of the VEGF biomarker remains somewhat higher than this value, which is not a great concern, since samples can be diluted before measurements. On the other hand, the analytical performance of the ellipsometry-based label-free sensor reported here, was found to be comparable with other methods. Moreover, both aptamers (anti-VEGF1 and anti-VEGF2) have selectively detected the VEGF and revealed a LOD value of about 5 pM which is a comparable value with the previously reported values. Also, it was re-supported using the kinetic data, that the interaction between aptamer and VEGF has occurred over the single binding site for both aptamers. Consequently, the detection sensitivity and selectivity of the VEGF sensor has been increased by developing a sensor based on spectroscopic ellipsometry and using aptamers with proven selectivity in this sensor.

Credit author statement

Mustafa Oğuzhan Çağlayan, Experiment, Methodology, Writing. Zafer Üstündağ, Experiment, Methodology, Formal analysis. İshak Afşin Kariper, Writing- Reviewing and Editing,

Declaration of competing interest

The authors declare that they have no known competing financial interests or personal relationships that could have appeared to influence

Table 5
Comparison of some aptamer-based VEGF sensors encountered in the relevant literature.

Method	Approach	Detection range	LOD	Ref.
Electrochemical	SPE decorated with Au nanoparticles, signal amplification via alkaline phosphatase, sandwich assay, aptamer	0–250 nM	30 nM	[67]
Electrochemical	Mesoporous carbon – Au nanoparticle decorated SPE, aptamer	0.5 pM–15 pM	0.05 pM	[80]
Electrochemical	Hemin, sandwich assay, aptamer	0–80 nM	1 nM	[81]
Electrochemical	Methylene blue, Au coated SPE, aptamer	0–20 pM	5 pM	[82]
FET	SiNW, FET, aptamer	104 pM–52 nM	104 pM	[51]
FET	Few layer graphene, nitrogen doped, made of poly (pyrrole), FET, RNA aptamer	100 fM- 10 nM	100 fM	[83]
FET	Functionalized poly (pyrrole) nanotube, FET, aptamer	400 fM – 4 μM	0.4 pM	[84]
Fluorescence	Au nanoparticle, fluorescence quenching, aptamer	1.25 pM–1.25 μM	1.25 pM	[42]
Fluorescence	Peptide nucleic acid immobilized beads, fluorescent dye, FRET, aptamer	5–50 nM	25 nM	[85]
Fluorescence	G-quadruplex aptamer – VEGF interaction, fluorescence polarization change	0.32–5 nM	0.32 nM	[78]
Fluorescence	Chemilimunescence resonance energy transfer (CRET), quantum dots, aptamer	0.875–87.5 nM	0.875 nM	[41]
Fluorescence	Eu(III)-chelate, quenching resonance energy transfer (QRET), aptamer	0.75–50 nM	0.25 nM	[86]
SERS	Silica coated hollow Au nanospheres, aptamer	5 pM–50 nM	0.5 pM	[87]
SERS	Ag decorated Au nanopyramids, aptamer	0.01–1.0 fM	22.6 aM	[88]
SPR	Carboxyl coated polystyrene microbeads, rolling circle amplification, aptamer	5 pM–50 nM	5 pM	[89]
SPR	A sandwich method, enzymatic amplification, RNA aptamer, and thrombin aptamer	NR	1 pM	[90]
Spectrophotometric ellipsometry	Aptamers immobilized on Si-wafer via MPTES, MUA, and EDAC routes.	10–1000 pM	5.81 pM 4.29 pM	This study

the work reported in this paper.

Acknowledgments

This study has been done between June 2019 and April 2020. The authors thank the Scientific Research Projects Division of Bilecik Seyh Edebali University (BŞEÜ-BAP, Bilecik, Turkey) for their supports and valuable grants under project number 2019-01.BŞEÜ.03-03.

References

[1] L. Wu, X. Qu, Cancer biomarker detection: recent achievements and challenges, Chem. Soc. Rev. 44 (2015) 2963–2997.
[2] O. Golubnitschaja, J. Flammer, What are the biomarkers for glaucoma? Surv. Ophthalmol. 52 (Suppl 2) (2007) S155–S161.
[3] C.L. Sawyers, The cancer biomarker problem, Nature 452 (2008) 548–552.
[4] K.J. Martin, M.V. Fournier, G.P. Reddy, A.B. Pardee, A need for basic research on fluid-based early detection biomarkers, Canc. Res. 70 (2010) 5203–5206.
[5] S.A. Kazane, D. Sok, E.H. Cho, M.L. Uson, P. Kuhn, P.G. Schultz, V.V. Smider, Site-specific DNA-antibody conjugates for specific and sensitive immuno-PCR, Proc. Natl. Acad. Sci. U. S. A 109 (2012) 3731–3736.
[6] D. Alberti, M. van't Erve, R. Stefania, M.R. Ruggiero, M. Tapparo, S. Geninatti Crich, S. Aime, A quantitative relaxometric version of the ELISA test for the measurement of cell surface biomarkers, Angew. Chem. 53 (2014) 3488–3491.
[7] J.E. Oesterling, Prostate specific antigen: a critical assessment of the most useful tumor marker for adenocarcinoma of the prostate, J. Urol. 145 (1991) 907–923.
[8] R.S. Gaster, D.A. Hall, C.H. Nielsen, S.J. Osterfeld, H. Yu, K.E. Mach, R.J. Wilson, B. Murmann, J.C. Liao, S.S. Gambhir, S.X. Wang, Matrix-insensitive protein assays push the limits of biosensors in medicine, Nat. Med. 15 (2009) 1327–1332.
[9] H. Lee, J.E. Park, J.M. Nam, Bio-barcode gel assay for microRNA, Nat. Commun. 5 (2014) 3367.
[10] S. Krishnan, V. Mani, D. Wasalathanthri, C.V. Kumar, J.F. Rusling, Attomolar detection of a cancer biomarker protein in serum by surface plasmon resonance using superparamagnetic particle labels, Angew. Chem. 50 (2011) 1175–1178.
[11] P.D. Howes, S. Rana, M.M. Stevens, Plasmonic nanomaterials for biodiagnostics, Chem. Soc. Rev. 43 (2014) 3835–3853.
[12] S.M. Tabakman, L. Lau, J.T. Robinson, J. Price, S.P. Sherlock, H. Wang, B. Zhang, Z. Chen, S. Tangsombatvisit, J.A. Jarrell, P.J. Utz, H. Dai, Plasmonic substrates for multiplexed protein microarrays with femtomolar sensitivity and broad dynamic range, Nat. Commun. 2 (2011) 466.
[13] H. Im, H. Shao, Y.I. Park, V.M. Peterson, C.M. Castro, R. Weissleder, H. Lee, Label-free detection and molecular profiling of exosomes with a nano-plasmonic sensor, Nat. Biotechnol. 32 (2014) 490–495.
[14] A. Samanta, K.K. Maiti, K.S. Soh, X. Liao, M. Vendrell, U.S. Dinish, S.W. Yun, R. Bhuvaneswari, H. Kim, S. Rautela, J. Chung, M. Olivo, Y.T. Chang, Ultrasensitive near-infrared Raman reporters for SERS-based in vivo cancer detection, Angew. Chem. 50 (2011) 6089–6092.
[15] G. Wu, R.H. Datar, K.M. Hansen, T. Thundat, R.J. Cote, A. Majumdar, Bioassay of prostate-specific antigen (PSA) using microcantilevers, Nat. Biotechnol. 19 (2001) 856–860.
[16] J. Wang, L. Wu, J. Ren, X. Qu, Visualizing human telomerase activity with primer-modified Au nanoparticles, Small 8 (2012) 259–264.
[17] B. Zhao, J. Yan, D. Wang, Z. Ge, S. He, D. He, S. Song, C. Fan, Carbon nanotubes multifunctionalized by rolling circle amplification and their application for highly sensitive detection of cancer markers, Small 9 (2013) 2595–2601.
[18] M. Labib, N. Khan, S.M. Ghobadloo, J. Cheng, J.P. Pezacki, M.V. Berezovski, Three-mode electrochemical sensing of ultralow microRNA levels, J. Am. Chem. Soc. 135 (2013) 3027–3038.
[19] L. Feng, L. Wu, J. Wang, J. Ren, D. Miyoshi, N. Sugimoto, X. Qu, Detection of a prognostic indicator in early-stage cancer using functionalized graphene-based peptide sensors, Adv. Mater. 24 (2012) 125–131.
[20] G.P. Smith, Filamentous fusion phage: novel expression vectors that display cloned antigens on the virion surface, Science (New York, N.Y.) 228 (1985) 1315–1317.
[21] S. Myung, A. Solanki, C. Kim, J. Park, K.S. Kim, K.B. Lee, Graphene-encapsulated nanoparticle-based biosensor for the selective detection of cancer biomarkers, Advanced materials (Deerfield Beach, Fla 23 (2011) 2221–2225.
[22] M.B. Lerner, J. D'Souza, T. Pazina, J. Dailey, B.R. Goldsmith, M.K. Robinson, A. T. Johnson, Hybrids of a genetically engineered antibody and a carbon nanotube transistor for detection of prostate cancer biomarkers, ACS Nano 6 (2012) 5143–5149.
[23] J. Wang, L. Wu, J. Ren, X. Qu, Visual detection of telomerase activity with a tunable dynamic range by using a gold nanoparticle probe-based hybridization protection strategy, Nanoscale 6 (2014) 1661–1666.
[24] S. Rana, A.K. Singla, A. Bajaj, S.G. Elci, O.R. Miranda, R. Mout, B. Yan, F.R. Jirik, V. M. Rotello, Array-based sensing of metastatic cells and tissues using nanoparticle-fluorescent protein conjugates, ACS Nano 6 (2012) 8233–8240.
[25] X. Wang, C. Wang, K. Qu, Y. Song, J. Ren, D. Miyoshi, N. Sugimoto, X. Qu, Ultrasensitive and selective detection of a prognostic indicator in early-stage cancer using graphene oxide and carbon nanotubes, Adv. Funct. Mater. 20 (2010) 3967–3971.
[26] D. Geissler, S. Stufler, H.G. Lohmannsroben, N. Hildebrandt, Six-color time-resolved Forster resonance energy transfer for ultrasensitive multiplexed biosensing, J. Am. Chem. Soc. 135 (2013) 1102–1109.
[27] C. Tuerk, L. Gold, Systematic evolution of ligands by exponential enrichment: RNA ligands to bacteriophage T4 DNA polymerase, Science (New York, N.Y.) 249 (1990) 505–510.
[28] A.D. Ellington, J.W. Szostak, In vitro selection of RNA molecules that bind specific ligands, Nature 346 (1990) 818–822.
[29] H. Liu, S. Xu, Z. He, A. Deng, J.J. Zhu, Supersandwich cytosensor for selective and ultrasensitive detection of cancer cells using aptamer-DNA concatamer-quantum dots probes, Anal. Chem. 85 (2013) 3385–3392.
[30] J. Yang, M. Palla, F.G. Bosco, T. Rindzevicius, T.S. Alstrom, M.S. Schmidt, A. Boisen, J. Ju, Q. Lin, Surface-enhanced Raman spectroscopy based quantitative bioassay on aptamer-functionalized nanopillars using large-area Raman mapping, ACS Nano 7 (2013) 5350–5359.

[31] A. Porchetta, A. Vallee-Belisle, K.W. Plaxco, F. Ricci, Using distal-site mutations and allosteric inhibition to tune, extend, and narrow the useful dynamic range of aptamer-based sensors, J. Am. Chem. Soc. 134 (2012) 20601–20604.
[32] E. Farjami, R. Campos, J.S. Nielsen, K.V. Gothelf, J. Kjems, E.E. Ferapontova, RNA aptamer-based electrochemical biosensor for selective and label-free analysis of dopamine, Anal. Chem. 85 (2013) 121–128.
[33] M. Labib, A.S. Zamay, O.S. Kolovskaya, I.T. Reshetneva, G.S. Zamay, R.J. Kibbee, S. A. Sattar, T.N. Zamay, M.V. Berezovski, Aptamer-based viability impedimetric sensor for bacteria, Anal. Chem. 84 (2012) 8966–8969.
[34] Q. Zhou, Y. Liu, D.S. Shin, J. Silangcruz, N. Tuleuova, A. Revzin, Aptamer-containing surfaces for selective capture of CD4 expressing cells, Langmuir : the ACS journal of surfaces and colloids 28 (2012) 12544–12549.
[35] M.R. Battig, B. Soontornworajit, Y. Wang, Programmable release of multiple protein drugs from aptamer-functionalized hydrogels via nucleic acid hybridization, J. Am. Chem. Soc. 134 (2012) 12410–12413.
[36] S.J. Lee, Y.S. Kwon, J.E. Lee, E.J. Choi, C.H. Lee, J.Y. Song, M.B. Gu, Detection of VR-2332 strain of porcine reproductive and respiratory syndrome virus type II using an aptamer-based sandwich-type assay, Anal. Chem. 85 (2013) 66–74.
[37] M. Famulok, J.S. Hartig, G. Mayer, Functional aptamers and aptazymes in biotechnology, diagnostics, and therapy, Chem. Rev. 107 (2007) 3715–3743.
[38] K. Hofer, L.V. Langejurgen, A. Jaschke, Universal aptamer-based real-time monitoring of enzymatic RNA synthesis, J. Am. Chem. Soc. 135 (2013) 13692–13694.
[39] C.R. Ireson, L.R. Kelland, Discovery and development of anticancer aptamers, Mol. Canc. Therapeut. 5 (2006) 2957–2962.
[40] D.A. Daniels, H. Chen, B.J. Hicke, K.M. Swiderek, L. Gold, A tenascin-C aptamer identified by tumor cell SELEX: systematic evolution of ligands by exponential enrichment, Proc. Natl. Acad. Sci. U. S. A 100 (2003) 15416–15421.
[41] R. Freeman, J. Girsh, A.F. Jou, J.A. Ho, T. Hug, J. Dernedde, I. Willner, Optical aptasensors for the analysis of the vascular endothelial growth factor (VEGF), Anal. Chem. 84 (2012) 6192–6198.
[42] H. Cho, E.C. Yeh, R. Sinha, T.A. Laurence, J.P. Bearinger, L.P. Lee, Single-step nanoplasmonic VEGF165 aptasensor for early cancer diagnosis, ACS Nano 6 (2012) 7607–7614.
[43] X. Chen, M.C. Estevez, Z. Zhu, Y.F. Huang, Y. Chen, L. Wang, W. Tan, Using aptamer-conjugated fluorescence resonance energy transfer nanoparticles for multiplexed cancer cell monitoring, Anal. Chem. 81 (2009) 7009–7014.
[44] J.K. Herr, J.E. Smith, C.D. Medley, D. Shangguan, W. Tan, Aptamer-conjugated nanoparticles for selective collection and detection of cancer cells, Anal. Chem. 78 (2006) 2918–2924.
[45] J. Yin, X. He, K. Wang, F. Xu, J. Shangguan, D. He, H. Shi, Label-free and turn-on aptamer strategy for cancer cells detection based on a DNA-silver nanocluster fluorescence upon recognition-induced hybridization, Anal. Chem. 85 (2013) 12011–12019.
[46] C.C. Huang, Y.F. Huang, Z. Cao, W. Tan, H.T. Chang, Aptamer-modified gold nanoparticles for colorimetric determination of platelet-derived growth factors and their receptors, Anal. Chem. 77 (2005) 5735–5741.
[47] S. Ye, Y. Yang, J. Xiao, S. Zhang, Surface-enhanced Raman scattering assay combined with autonomous DNA machine for detection of specific DNA and cancer cells, Chem Commun (Camb) 48 (2012) 8535–8537.
[48] L. Feng, Y. Chen, J. Ren, X. Qu, A graphene functionalized electrochemical aptasensor for selective label-free detection of cancer cells, Biomaterials 32 (2011) 2930–2937.
[49] Y. Zhu, P. Chandra, Y.B. Shim, Ultrasensitive and selective electrochemical diagnosis of breast cancer based on a hydrazine-Au nanoparticle-aptamer bioconjugate, Anal. Chem. 85 (2013) 1058–1064.
[50] F. Ma, C. Ho, A.K.H. Cheng, H.-Z. Yu, Immobilization of redox-labeled hairpin DNA aptamers on gold: electrochemical quantitation of epithelial tumor marker mucin 1, Electrochim. Acta 110 (2013) 139–145.
[51] H.S. Lee, K.S. Kim, C.J. Kim, S.K. Hahn, M.H. Jo, Electrical detection of VEGFs for cancer diagnoses using anti-vascular endotherial growth factor aptamer-modified Si nanowire FETs, Biosens. Bioelectron. 24 (2009) 1801–1805.
[52] R.A. Gatenby, R.J. Gillies, A microenvironmental model of carcinogenesis, Nat. Rev. Canc. 8 (2008) 56–61.
[53] W. Liu, J. Xu, M. Wang, Q. Wang, Y. Bi, M. Han, Tumor-derived vascular endothelial growth factor (VEGF)-a facilitates tumor metastasis through the VEGF-VEGFR1 signaling pathway, Int. J. Oncol. 39 (2011) 1213–1220.
[54] A. Hoeben, B. Landuyt, M.S. Highley, H. Wildiers, A.T. Van Oosterom, E.A. De Bruijn, Vascular endothelial growth factor and angiogenesis, Pharmacol. Rev. 56 (2004) 549–580.
[55] G. McMahon, VEGF receptor signaling in tumor angiogenesis, Oncol. 5 (Suppl 1) (2000) 3–10.
[56] N. Ferrara, Vascular endothelial growth factor: basic science and clinical progress, Endocr. Rev. 25 (2004) 581–611.
[57] R. Roskoski Jr., Vascular endothelial growth factor (VEGF) signaling in tumor progression, Crit. Rev. Oncol.-Hematol. 62 (2007) 179–213.
[58] P. Carmeliet, R.K. Jain, Angiogenesis in cancer and other diseases, Nature 407 (2000) 249–257.
[59] K.H. Plate, G. Breier, H.A. Weich, W. Risau, Vascular endothelial growth factor is a potential tumour angiogenesis factor in human gliomas in vivo, Nature 359 (1992) 845–848.
[60] P. Salven, A. Orpana, H. Joensuu, Leukocytes and platelets of patients with cancer contain high levels of vascular endothelial growth factor, Clin. Canc. Res. : an official journal of the American Association for Cancer Research 5 (1999) 487–491.
[61] A. Mitsuhashi, K. Suzuka, K. Yamazawa, H. Matsui, K. Seki, S. Sekiya, Serum vascular endothelial growth factor (VEGF) and VEGF-C levels as tumor markers in patients with cervical carcinoma, Cancer 103 (2005) 724–730.
[62] R.T. Poon, C.P. Lau, S.T. Cheung, W.C. Yu, S.T. Fan, Quantitative correlation of serum levels and tumor expression of vascular endothelial growth factor in patients with hepatocellular carcinoma, Canc. Res. 63 (2003) 3121–3126.
[63] J. Zhao, F. Yan, H. Ju, J. Tang, J. Qin, Correlation between serum vascular endothelial growth factor and endostatin levels in patients with breast cancer, Canc. Lett. 204 (2004) 87–95.
[64] H. Nakahara, J. Song, M. Sugimoto, K. Hagihara, T. Kishimoto, K. Yoshizaki, N. Nishimoto, Anti-interleukin-6 receptor antibody therapy reduces vascular endothelial growth factor production in rheumatoid arthritis, Arthritis Rheum. 48 (2003) 1521–1529.
[65] M. Detmar, Evidence for vascular endothelial growth factor (VEGF) as a modifier gene in psoriasis, J. Invest. Dermatol. 122 (2004) xiv–xv.
[66] D. Ray, M. Mishra, S. Ralph, I. Read, R. Davies, P. Brenchley, Association of the VEGF gene with proliferative diabetic retinopathy but not proteinuria in diabetes, Diabetes 53 (2004) 861–864.
[67] A. Ravalli, L. Rivas, A. De la Escosura-Muniz, J. Pons, A. Merkoci, G. Marrazza, A DNA aptasensor for electrochemical detection of vascular endothelial growth factor, J. Nanosci. Nanotechnol. 15 (2015) 3411–3416.
[68] H.G. Tompkins, P.H. Williams, Five layer stack of nitride, oxide, and amorphous silicon on glass, analyzed with spectroscopic ellipsometry, J. Vac. Sci. Technol. 15 (1997) 992–997.
[69] W.M. Duncan, S.A. Henck, Insitu spectral ellipsometry for real-time measurement and control, Appl. Surf. Sci. 63 (1993) 9–16.
[70] E. Garcia-Caurel, A. Martino, J.-P. Gaston, L. Yan, Focal point review - application of spectroscopic ellipsometry and mueller ellipsometry to optical characterization, Appl. Spectrosc. Rev. 67 (2013) 1–21.
[71] J.A. Woollam, P.G. Snyder, Fundamentals and applications of variable angle spectroscopic ellipsometry, Mater. Sci. Eng., B 5 (1990) 279–283.
[72] H.G. Tompkins, T. Zhu, E. Chen, Determining thickness of thin metal films with spectroscopic ellipsometry for applications in magnetic random-access memory, J. Vac. Sci. Technol. 16 (1998) 1297–1302.
[73] M.O. Caglayan, Aptamer-based ellipsometric sensor for ultrasensitive determination of aminoglycoside group antibiotics from dairy products, J. Sci. Food Agric. 100 (2020) 3386–3393.
[74] M.O. Caglayan, Z. Üstündağ, Spectrophotometric ellipsometry based Tat-protein RNA-aptasensor for HIV-1 diagnosis, Spectrochim. Acta Mol. Biomol. Spectrosc. 227 (2020) 117748.
[75] A. Keske, A. Atar, Üstünda, lknur, ça, M.O. layan, Uzhan, detection of Influenza A by surface plasmon resonance enhanced total internal reflection ellipsometry, J. Comput. Theor. Nanosci. 11 (2014) 981–986.
[76] M.O. Caglayan, Plasmon resonance-enhanced internal reflection ellipsometry for the trace detection of mercuric ion, Int. J. Environ. Sci. Technol. 15 (2018) 909–914.
[77] M.O. Caglayan, Z. Üstündağ, Detection of zearalenone in an aptamer assay using attenuated internal reflection ellipsometry and it's cereal sample applications, Food Chem. Toxicol. 136 (2020) 111081.
[78] S.-E. Wang, Y. Huang, K. Hu, J. Tian, S. Zhao, A highly sensitive and selective aptasensor based on fluorescence polarization for the rapid determination of oncoprotein vascular endothelial growth factor (VEGF), Anal. Methods 6 (2014) 62–66.
[79] Y. Nonaka, K. Sode, K. Ikebukuro, Screening and improvement of an anti-VEGF DNA aptamer, Molecules 15 (2010).
[80] M. Amouzadeh Tabrizi, M. Shamsipur, L. Farzin, A high sensitive electrochemical aptasensor for the determination of VEGF(165) in serum of lung cancer patient, Biosens. Bioelectron. 74 (2015) 764–769.
[81] Z. Lv, K. Wang, X. Zhang, A new electrochemical aptasensor for the analysis of the vascular endothelial growth factor, J. Immunoassay Immunochem. 35 (2014) 233–240.
[82] S. Zhao, W. Yang, R.Y. Lai, A folding-based electrochemical aptasensor for detection of vascular endothelial growth factor in human whole blood, Biosens. Bioelectron. 26 (2011) 2442–2447.
[83] O.S. Kwon, S.J. Park, J.-Y. Hong, A.R. Han, J.S. Lee, J.S. Lee, J.H. Oh, J. Jang, Flexible FET-type VEGF aptasensor based on nitrogen-doped graphene converted from conducting polymer, ACS Nano 6 (2012) 1486–1493.
[84] O.S. Kwon, S.J. Park, J. Jang, A high-performance VEGF aptamer functionalized polypyrrole nanotube biosensor, Biomaterials 31 (2010) 4740–4747.
[85] C. Mita, K. Abe, T. Fukaya, K. Ikebukuro, Vascular endothelial growth factor (VEGF) detection using an aptamer and PNA-based bound/free separation system, Materials 7 (2014) 1046–1054.
[86] K. Kopra, M. Syrjanpaa, P. Hanninen, H. Harma, Non-competitive aptamer-based quenching resonance energy transfer assay for homogeneous growth factor quantification, Analyst 139 (2014) 2016–2023.
[87] J. Ko, S. Lee, E.K. Lee, S.I. Chang, L. Chen, S.Y. Yoon, J. Choo, SERS-based immunoassay of tumor marker VEGF using DNA aptamers and silica-encapsulated hollow gold nanospheres, Phys. Chem. Chem. Phys. 15 (2013) 5379–5385.

[88] S. Zhao, W. Ma, L. Xu, X. Wu, H. Kuang, L. Wang, C. Xu, Ultrasensitive SERS detection of VEGF based on a self-assembled Ag ornamented–AU pyramid superstructure, Biosens. Bioelectron. 68 (2015) 593–597.
[89] H. Chen, Y. Hou, F. Qi, J. Zhang, K. Koh, Z. Shen, G. Li, Detection of vascular endothelial growth factor based on rolling circle amplification as a means of signal enhancement in surface plasmon resonance, Biosens. Bioelectron. 61 (2014) 83–87.
[90] Y. Li, H.J. Lee, R.M. Corn, Detection of protein biomarkers using RNA aptamer microarrays and enzymatically amplified surface plasmon resonance imaging, Anal. Chem. 79 (2007) 1082–1088.